# MODELLING DELAMINATION OF TI-CFRP INTERFACES

E. Savani[1], A. Pirondi[1*], F. Carta[1], A.C. Nogueira[2], E. Hombergsmeier[3]

[1] *Dipartimento di Ingegneria Industriale, Università di Parma, Parco Area delle Scienze 181/A, 43124 Parma, Italy*
[2] *Fraunhofer Institute for Chemical Technology, Universitätsstrasse 1a, 86159, Augsburg, Germany*
[3]*Metallic Technologies & Surface Engineering, EADS Innovation Works, Willy-Messerschmitt Straße, 85521 Ottobrunn, Germany*
**alessandro.pirondi@unipr.it*

**Keywords:** cohesive zone model, Ti-CFRP co-bonds, composite joints, local Ti reinforcements

## Abstract
*The aim of the investigations is to identify numerically the cohesive zone parameters of Ti-CFRP interfaces, in the future perspective of simulating the strength of composite joints with local Ti reinforcements. Ti-CFRP co-cured specimens have been tested experimentally and were then simulated with FEA in order to identify the cohesive zone parameters of the Ti-CFRP interface. Two different combinations of fiber orientation with respect to the crack plane (0° and 90°) were considered, as well as two different stacking sequences, i.e. Ti plates co-cured with two CFRP plies in the middle and, vice-versa, CFRP adherends co-cured with a thin Ti lamina in the middle.*

## 1 Introduction
### *1.1 Ti-CFRP interfaces in composite laminate joining*
The joining of composite laminates is generally made by mechanical fastening or bonding, as testified from the large number of studies on that [1]. Fastening ensures the possibility of decoupling and it is of simple inspection, however the drilling of a hole through the composite affects the fiber continuity and therefore the bearing and shear strength of the component.
As fiber-metal laminates (FML) are known to bring toghether the advantages of of high strength/weight ratio of a fiber-reinforced polymer with the ductility and toughness of a metal, they are more indicated to sustain bearing in fastened connections. Titanium is especially suited as a metallic ply because of its high strength over weight ratio, high specific stiffness, excellent mechanical behaviour in harsh conditions as high temperature and wet environment, giving raise to the so-called Hybrid Titanium Composite Laminate (HTCL). Titanium is generally used where its benefit is maximum, i.e. in the bolt hole area, as shown in Fig. 1.

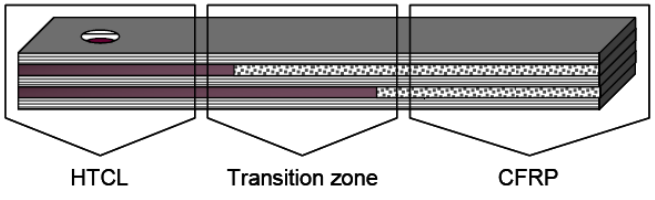


**Figure 1.** Outline of a HTCL used as a reinforcement in the bolt hole area.

Bearing failure of HTCL fastened joints involves all of the possible damage mechanisms as CFRP fiber and matrix failure, Ti plastic deformation and failure, Ti-CFRP delamination [2]. The bearing failure of HTCL fastened connections has been modeled in detail in [3, 4], showing that the modelling of Ti-CFRP delamination in both the bolt hole and transition regions is necessary to obtain a good correspondence between experiments and simulations. It is worth to underline that both papers, as many others in the field composite delamination modelling, make use of the cohesive zone model to predict delamination, for which it is necessary to introduce properly identified cohesive parameters.
On the other hand, when composite laminates are joined by bonding or co-curing, the joint strength is typically limited by the onset of debonding and/or delamination. In order to improve debonding/delamination resistance, techniques such as Z-anchoring, stitching, tufting or Z-pinning (Fig. 2, [5]) can be considered, and in particular the latter [6].

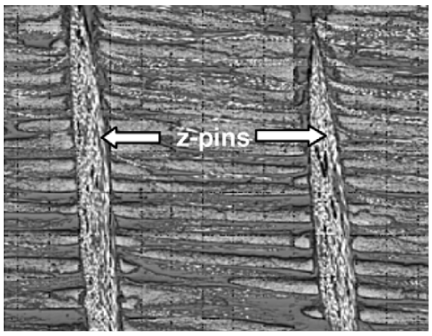


**Figure 2.** Outline of Z-pins in a composite laminate [5]. Pin diameter is typically in the 0.1-1.0 mm range.

The mechanism behind Z-pinning debonding/delamination strength improvement has been studied and simulated in several works [7-13], where in the majority of cases Z-pins were made of UD carbon-fiber composite, while Ti rods were also considered for example in [10]. Recently, the possibility of forming metallic pins on metallic parts by "cold-metal transfer" technology has been shown [14], along with the possibility of obtaining different pinhead shapes. In this way, it is possible to Z-pin the co-cured adhesive bond between a metallic and composite part, Fig. 3.

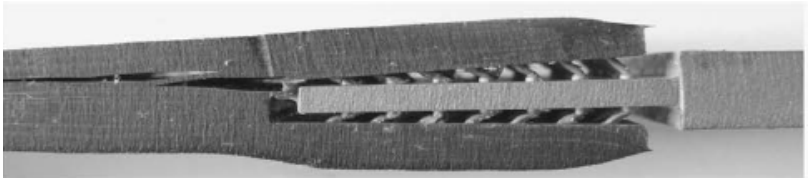

**Figure 3.** Example of Z-pinned metal-composite joint by cold-metal transfer manufactured pins [10].

The concept of Z-pinning has been further evolved in the work of [15], where 3D interlocking of CFRP laminates co-bonded structures is achieved through the employment of Z-pins obtained by shearing and folding of thin metal sheets, which are then placed between the composite parts before curing.
Alike HTCL reinforcement of bolt holes, also in the case of Z-pinning, and especially in hybrid techniques like those presented in [14, 15], composite-metal delamination is an important mechanism to be considered in failure modelling. Again, the use of the cohesive zone model, for which it is necessary to introduce properly identified cohesive parameters is the basic tool to predict delamination.
The investigation done in this work is therefore aimed at identifying numerically the cohesive zone parameters of Ti-CFRP interfaces, in the perspective of simulating the strength of

composite joints with local Ti reinforcements. Ti-CFRP co-cured specimens have been tested experimentally and were then simulated with FEA in order to identify the cohesive zone parameters of the Ti-CFRP interface. Two different combinations of fiber orientation with respect to the crack plane (0° and 90°) were considered, as well as two different stacking sequences, i.e. Ti plates co-cured with two CFRP plies in the middle and, vice-versa, CFRP adherends co-cured with a thin Ti lamina in the middle.

*1.2 Cohesive zone model*

The origin of the cohesive zone model (CZM) can be dated back to the work of Dugdale and Barrenblatt in the '60 to describe the plastic zone at the crack tip in thin metallic sheets. Since it is essentially a very simple and general description of the stresses in a strip ahead of the crack tip, it has been later used as a micromechanical model for the simulation of the quasi static crack growth problems, especially in the case of interface cracks such as delamination in composites and bonded joints. The relationship between the tensile/shear stress (σ) and the opening/sliding (δ) of crack faces at the crack tip is of the kind represented in Figure 4 and it is simulated with finite element analysis (FEA) by assigning a specific traction-separation behaviour at the so called cohesive elements placed ahead of the crack.

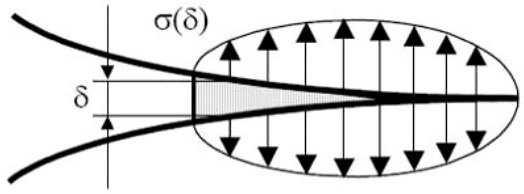


**Figure 1.** Cohesive stresses at the crack tip.

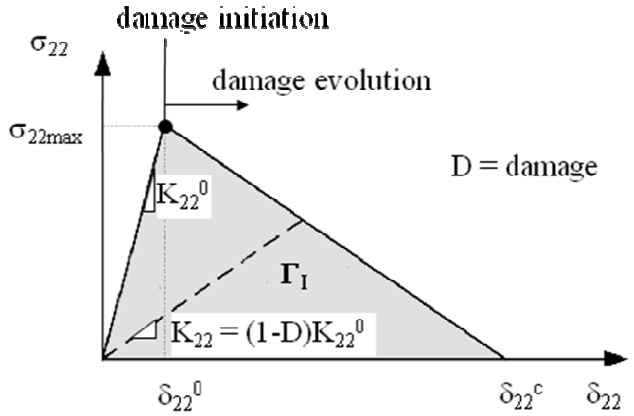


**Figure 2.** Example of a linear damage cohesive law.

The traction-separation behavior assigned to cohesive elements is represented in Figure 5 for example by a triangular law. The elements initially behaves linearly. When a certain level of displacement (or stress) is reached, the stiffness and strength are progressively reduced until the complete separation is obtained. More complicated shapes, such as trapezoidal or exponential decay laws, were also developed to better describe the fracture where necessary.

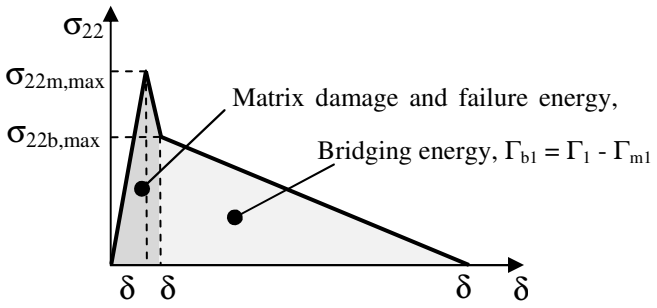


**Figure 6.** Schematic mode I traction–separation law used to describe fracture of composite with fiber bridging. The peak load corresponds to matrix cracking, followed by fiber pull-out [16].

In the case of composite-composite or metal-composite joint fracture, or composite delamination, the cohesive law can be broken up into two components, associated with matrix

cracking and with fiber bridging, respectively (Fig. 6), which has been shown more appropriate in describing the experimental behavior than a simple linear damage law such as the one in Fig. 5 [16].

## 2 Materials and testing methods

### *2.1 Ti-CFRP-Ti specimens*

The specimens are made by two Ti-6Al-4V, 252x25x2.95 $mm^3$ plates interleaved by two 252x25x0.125 $mm^3$ pre-preg M21-T800 UD plies, placed at 0° with respect to the crack propagation direction in one series and at 90° in another series. A 25x25x0.02 $mm^3$ kapton tape is placed between Ti and composite in order to create an initial (25 mm long) delamination. Mode I and Mode II fracture testing have been performed at EADS Innovation Works (Ottobrunn, Germany) according to Airbus AITM 1-0005 (Mode I) and AITM 1-0006 (Mode II). A fatigue precrack has been done before testing.

### *2.2 CFRP-Ti-CFRP specimens*

The specimens are made by two CFRP adherends, which dimensions of 252x25x2 $mm^3$ are obtained using 16 pre-preg M21-T800 UD plies, interleaved by a 252x25x0.2 $mm^3$ thick Ti-6Al-4V plate. The UD plies are placed at 0° with respect to the crack propagation direction, since a 90° placement would result a too weak adherend. A 25x25x0.02 $mm^3$ kapton tape is placed between Ti and composite in order to create an initial crack. Mode I and Mode II fracture testing have been performed at EADS Innovation Works (Ottobrunn, Germany) according to Airbus AITM 1-0005 (Mode I) and AITM 1-0006 (Mode II). A static precrack has been created before testing.

## 3 Cohesive zone parameters identification

### *3.1 FE modelling*

The FE models of mode I and mode II tests are shown in Fig. 7. Eight-node solid elements are used to model Ti adherends while continuum shell elements were used for CFRP. The crack propagation is allowed through the use of solid cohesive elements with no physical thickness placed at one of the two interfaces between Ti and CFRP, the other interface is given instead a rigid kinematic constraint (tie).

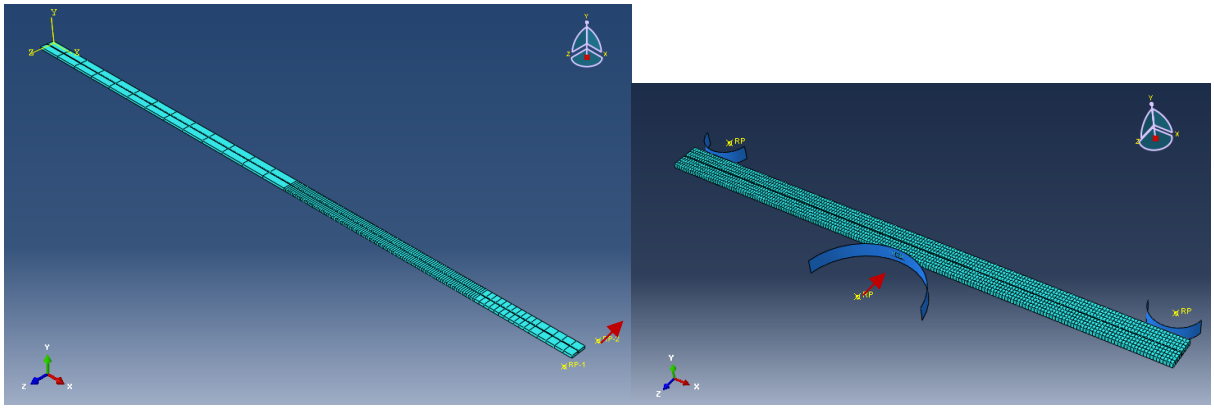

**Figure 7.** FE model of the mode I (left) and mode II (right) specimens.

The size of the cohesive elements is 0.2 mm in the region of crack propagation, as obtained from an initial mesh dependence analysis. The cohesive behavior is represented by a traction-separation law with strain calculation thickness of 1 mm. Concerning the adherends, in mode I one element through the thickness was enough to ensure mesh independence, while in the mode II case four elements were necessary. The entire geometry is modeled to account for the

slight asymmetry in the adherends, as explained in 2.1 and 2.2. In order to reduce the computation time, the width is reduced to 1 mm. Kinematic constraints of the kind "plane-remains-plane" are attributed to the lateral faces, allowing for uniform contraction or dilatation in order to approximate the real thicknes without enforcing plane strain.
The boundary conditions are applied to the reference points shown in Fig. 7, which are located in the same position as in the experiments. Analytical rigid surfaces simulate the steel pins of the three-point-bending device used in mode II. The elastic constants concerning Ti and CFRP, supplied by EADS Innovation Works, are summarized in Tab. 1. Plasticity (Ti), damage and failure (CFRP) characterization were also available but, from preliminary analyses, it was shown that adherends remain elastic and undamaged.
Automatic, adaptive stabilization of the solution was used, with a viscous dissipation factor of 2e-6 and a maximum ratio of viscous stabilization energy/strain energy of 5e-5.

*isotropic material behavior

| | $E_{11}$ | $E_{22}$ | $E_{33}$ | $\nu_{12}$ | $\nu_{13}$ | $\nu_{23}$ | $G_{12}$ | $G_{13}$ | $G_{23}$ |
|---|---|---|---|---|---|---|---|---|---|
| **CFRP** | 157000 | 10000 | 10000 | 0.3 | 0.3 | 0.45 | 5000 | 5000 | 3000 |
| **Titanium*** | 107000 | - | - | 0.3 | - | - | - | - | - |

**Table 1.** elastic constants used in FE analysis.

*3.2 Cohesive parameters identification*
The identification started from mode I, considering the linear damage law of Fig. 5. The initial stiffness $K_{22}^0$ was determined by increasing progressively the value until the FE trend coincided with the elastic trend experimental of the experiments. Once established the stiffness, a value of $\sigma_{22,max}$ was determined by fixing the cohesive energy $\Gamma_1 = G_{Ic}$, then increasing progressively $\sigma_{22,max}$ until little, if no deviation from linearity was left before the force peak. Finally the cohesive energy $\Gamma_1$ was varied until a good convergence was found on the post-peak force trend until openings of about 5 mm.. The same procedure was used also in the case of mode II, where the correspondence between simulation and experiments was cheked up to deflections of about 2 mm. Since large crack propagations (up to 60-70 mm) accompanied by fiber bridging are expected in mode I, the bi-linear damage law shown in Fig. 6 has been also considered. In this case, $K_{22}^0$ and $\sigma_{22m,max}$ are determined in the same way as for the linear damage law. The value of $\sigma_{22b,max}$, $\Gamma_{m1}$ and $\Gamma_1$ are then identified by trial-and-error in order to reproduce more closely the data in the post-force peak phase.

## 4 Results and discussion

*4.1 Ti-CFRP-Ti mode I cohesive zone parameters*
The result of identification is shown in Fig. 8a-b. For the sake of clarity, only one representative experiment is shown. In the case of the linear damage law, the overall trend is caught, with an overestimation of the force peak of 6-12%. The value of $\Gamma_1$ necessary to obtain such correlation is 0.5 N/mm (0°) and 0.58 N/mm (90°), which is much lower than $G_{Ic}$ = 0.78 N/mm (0°) or 1.04 N/mm (90°). Using the bi-linear damage law, an even better correlation is found, where now the post peak trend is more faithfully reproduced. The motivation is, as explained in 1.1, that the bi-linear damage law is representative of the fiber bridging which may occur in composite joints, with an extent depending on the type of composite material. In this way, the value of $\Gamma_1$ increases to 0.58 N/mm (0°) and 0.62 N/mm (90°), respectively. The reason for this discrepancy is found in the way $G_{Ic}$ is evaluated from experiments. In fact, AITM 1-0005 contemplates that $G_{Ic}$ is calculated according to Fig. 9, that is an average value over the whole crack propagation span, which in this case is around 65 mm (from $a_i$ about 35 mm to a final length $a_f$ of 100 mm as prescribed by AITM 1-0005).

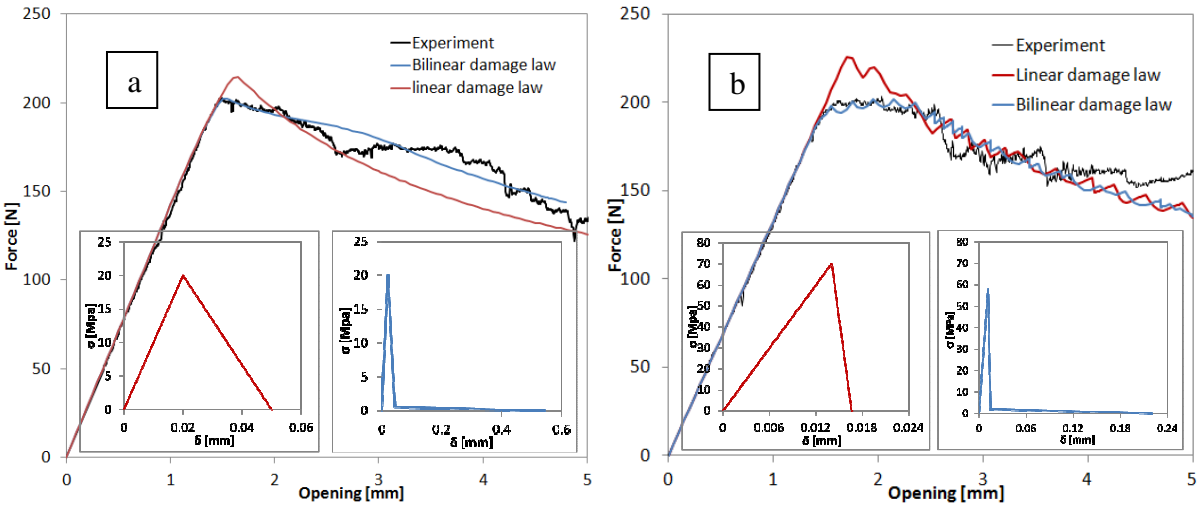


**Figure 8.** Comparison betw. experiment and simulations (Ti-CFRP-Ti). Ply orientation: a) 0°; b) 90°.

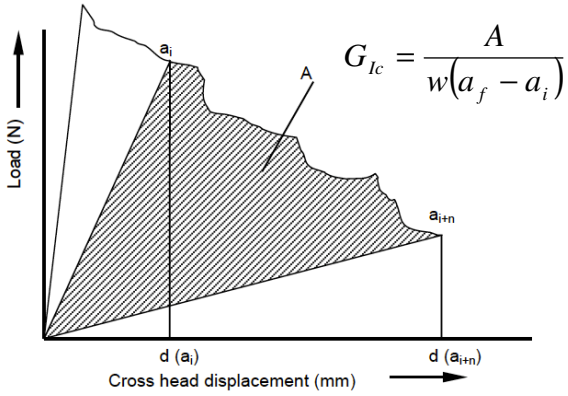


**Figure 9.** $G_{Ic}$ evaluation according to AITM 1-0005 procedure.

According for example to the beam on elastic foundation solution of [17]:

$$G_{Ic} = \frac{P^2 a_i^{\,2}}{bE_{Ti}I}\left(1+\frac{1}{\lambda_\sigma a_i}\right)^2 ;\ \lambda_\sigma = \left(\frac{6}{h^3 t}\frac{E_{33comp}}{E_{Ti}}\right)^{1/4} \quad (1)$$

where t is the thickness of the CFRP laminae (t = 0.25mm), I the area moment of inertia of the titanium plate, b and h plate width and thickness, respectively. If $G_{Ic}$ was evaluated using Eqn. (1) and the values of $P_{max}$ and $a_i$, a value of 0.46 N/mm would have been found for the tests represented in Fig. 8, which is closer to the value of $\Gamma_1$ used in the simulation. From this analysis, we may guess that the value of $G_{Ic}$ increases with crack propagation and justifies the discrepancy between the value calculated according to the AITM procedure and $\Gamma_1$, which is identified using only the first millimeters of propagation.

*4.2 Ti-CFRP-Ti mode II cohesive zone parameters*

The result of identification is shown in Fig. 10a-b for 0° and 90° ply orientation. In this case, as fiber bridging should be of minor importance than in mode I, only a linear damage law has been used. As in the mode I case, the laws identified are quite different from each other depending of fiber orientation. However, in this case the value of $\Gamma_2$ is 1.18 N/mm (0°) and 1.34 N/mm (90°), which fits closely to $G_{IIc}$ (1.36 N/mm at 0° and 1.34 N/mm at 90°). In this

case, the crack propagation is only a few millimeters, therefore the cohesive law is identified on the whole propagation span and this is reason of the consistency between $\Gamma_2$ and $G_{IIc}$.

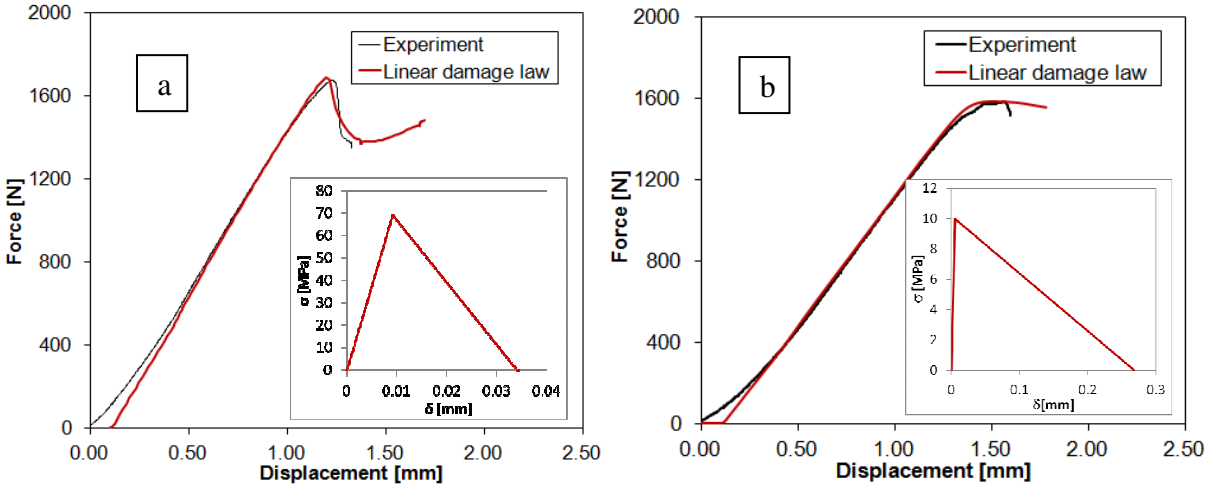


**Figure 10.** Comparison betw. experiment and simulations (Ti-CFRP-Ti). Ply orientation: a) 0°; b) 90°.

*4.3 CFRP-Ti-CFRP mode I cohesive zone parameters*

The cohesive zone parameters have been identified in Fig. 11 for mode I. In this case, given the results obtained in 4.1, a bi-linear damage law has been used for mode I and a linear one for mode II. The corresponding value of $\Gamma_1$ is 0.99 N/mm, which is practically coincident with the experimental one (1 N/mm, evaluated as the average over 72 mm of propagation). It is worth to notice that the application of Eqn. (1) using $P_{max}$ and $a_i$ yields in this case a value $G_{Ic}$ =1.04 N/mm, meaning that there is no toughening with crack propagation, differently from Ti-CFRP-Ti specimens. However, the value of $G_{Ic}$ is in this case is higher than in Ti-CFRP-Ti (about 1/3 with respect to the average value over the propagation span and twice the initiation value), which brings in the necessity of further investigation on the fracture mechanism.

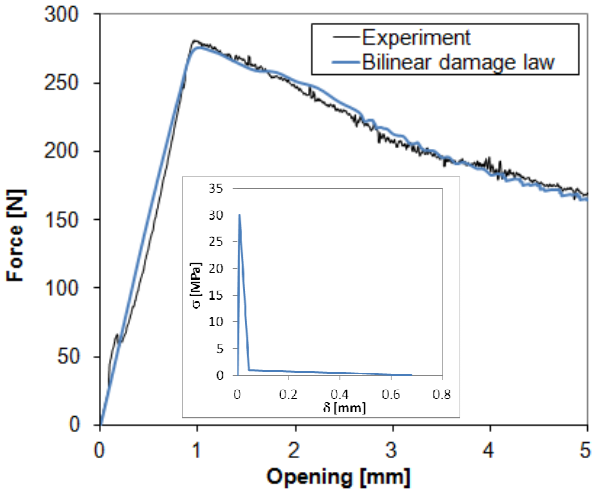


**Figure 11.** Comparison betw. experiment and simulations (Ti-CFRP-Ti).

## Conclusions

The investigations done in this work allowed the identification of the cohesive zone parameters of Ti-CFRP interfaces, in the perspective of simulating the strength of composite joints with local Ti reinforcements. The fundamental results are:

- mode I fracture of Ti-CFRP-Ti specimens is reproduced better using a bi-linear damage law instead of a linear one;

- the increase of $G_{Ic}$ shown by Ti-CFRP-Ti for long crack propagations cannot be caught by the model, where only short crack propagations are simulated for computational reasons;
- mode II fracture of Ti-CFRP-Ti specimens is well approximated by using a linear damage law, differently from mode I. the explanation is found in the lower extent of fiber bridging with respect to mode I fracture;
- the mode I CFRP-Ti-CFRP case requires a higher cohesive energy than Ti-CFRP-Ti one, justified by a higher mode I fracture toughness. Also in this case, the fracture behavior is reproduced better using a bi-linear damage law instead of a linear one.

**References**

[1] Camanho P.P., Tong L., Eds. *Composite Joints and Connections*. Woodhead Publishing, Cambridge, UK (2001).
[2] Kolesnikov B., Herbeck L., Fink A. CFRP/titanium hybrid material for improving composite bolted joints. *Composite Structures*, **83**, pp. 368-380 (2008).
[3] Camanho P.P., Fink A., Obst A., Pimenta S. Hybrid titanium-CFRP laminates for high performance bolted joints. *Composites: Part A*, **40**, pp. 1826-1837 (2009).
[4] Vermeer P., Eleuteri M., Pirondi A., Alderliesten R.C., Nogueira-da-Silva A.C. *Experimental and FEM investigation on the bearing properties of hybrid titanium composite laminates* in "Proceedings of *ICCS 16*", Porto, Portugal, (2011).
[5] Lander J.K. *Designing with z-pins: locally reinforced composite structures*. PhD Thesis, Cranfield University, Cranfield, UK (2008).
[6] Mouritz A.P. Review of z-pinned composite laminates. *Composites: Part A*, **38**, pp. 2383-2397 (2007).
[7] Yan W., Liu H.-Y., Mai Y.-W. Numerical study on the mode I delamination toughness of z-pinned laminates. *Composite Science and Technology*, **63**, pp. 1481-1493 (2003).
[8] Grassi M., Zhang X. Finite element analyses of mode I interlaminar delamination in z-fibre reinforced composite laminates *Composite Science and Technology*, **63**, pp. 1815-1832 (2003).
[9] Yan W., Liu H.-Y., Mai Y.-W. Mode II delamination toughness of z-pinned laminates. *Composite Science and Technology*, **64**, pp. 1937-1945 (2004).
[10] Cartié D.D.R., Cox B.N., Fleck N.A. Mechanisms of crack bridging by composite and metallic rods *Composites: Part A*, **35**, pp. 1325-1336 (2004).
[11] Dantuluri V., Maiti S., Geubelle P.H., Patel R., Kilic H. Cohesive modeling of delamination in Z-pin reinforced composite laminates. *Composite Science and Technology*, **67**, pp. 616-631 (2007).
[12] Bianchi F., Zhang X. A cohesive zone model for predicting delamination suppression in z-pinned laminates *Composite Science and Technology*, **71**, pp. 1898-1907 (2011).
[13] Bianchi F., Zhang X. Predicting mode II delamination suppression in z-pinned laminates *Composite Science and Technology*, **72**, pp. 924-932 (2012).
[14] Ucsnik S., Scheerer M., Zaremba S., Pahr D.H. Experimental investigation of a novel hybrid metal–composite joining technology *Composites: Part A*, **41**, pp. 369-374 (2010).
[15] Nogueira-da-Silva A.C., Drechsler K., Hombergsmeier E., Furfari D., Pacchione M. *Investigation of a hybrid 3D-reinforced joining technology for lightweight structures* in "Proceedings of *ICCS 16*", Porto, Portugal, (2005).
[16] Li S., Thouless M.D., Waas A.M., Schroeder J.A., Zavattieri P.D. Use of a cohesive-zone model to analyze the fracture of a fiber-reinforced polymer–matrix composite *Composite Science and Technology*, **65**, pp. 537-549 (2011).
[17] Krenk, S. Energy release rate of symmetric adhesive joints. *Engineering Fracture Mechanics*. **43**(4), pp. 549-559 (1992).